Atmos. Chem. Phys., 14, 7573–7583, 2014
www.atmos-chem-phys.net/14/7573/2014/
doi:10.5194/acp-14-7573-2014

Atmospheric Chemistry and Physics
Open Access

3-D model simulations of dynamical and microphysical interactions in pyroconvective clouds under idealized conditions

P. Reutter[1,2], J. Trentmann[3], A. Seifert[3], P. Neis[1,2], H. Su[1], D. Chang[1], M. Herzog[4], H. Wernli[5], M. O. Andreae[1], and U. Pöschl[1]

[1]Max Planck Institute for Chemistry, Biogeochemistry and Multiphase Chemistry Departments, Mainz, Germany
[2]Institute for Atmospheric Physics, Johannes Gutenberg-University, Mainz, Germany
[3]Deutscher Wetterdienst, DWD, Offenbach, Germany
[4]Department of Geography, University of Cambridge, Cambridge, UK
[5]ETH Zurich, Zurich, Switzerland

Correspondence to: P. Reutter (preutter@uni-mainz.de)

Received: 28 June 2013 – Published in Atmos. Chem. Phys. Discuss.: 23 July 2013
Revised: 5 June 2014 – Accepted: 18 June 2014 – Published: 29 July 2014

Abstract. Dynamical and microphysical processes in pyroconvective clouds in mid-latitude conditions are investigated using idealized three-dimensional simulations with the Active Tracer High resolution Atmospheric Model (ATHAM). A state-of-the-art two-moment microphysical scheme building upon a realistic parameterization of cloud condensation nuclei (CCN) activation has been implemented in order to study the influence of aerosol concentration on cloud development. The results show that aerosol concentration influences the formation of precipitation. For low aerosol concentrations ($N_{CN} = 200\,cm^{-3}$), rain droplets are rapidly formed by autoconversion of cloud droplets. This also triggers the formation of large graupel and hail particles, resulting in an early onset of precipitation. With increasing aerosol concentration ($N_{CN} = 1000\,cm^{-3}$ and $N_{CN} = 20\,000\,cm^{-3}$) the formation of rain droplets is delayed due to more but smaller cloud droplets. Therefore, the formation of ice crystals and snowflakes becomes more important for the eventual formation of graupel and hail, which is delayed at higher aerosol concentrations. This results in a delay of the onset of precipitation and a reduction of its intensity with increasing aerosol concentration. This study is the first detailed investigation of the interaction between cloud microphysics and the dynamics of a pyroconvective cloud using the combination of a high-resolution atmospheric model and a detailed microphysical scheme.

1 Introduction

Deep convection induced by vegetation fires is one of the most intense forms of atmospheric convection. The extreme cloud dynamics with high updraft velocities up to $20\,m\,s^{-1}$ (Trentmann et al., 2006; Rosenfeld et al., 2007; Reutter et al., 2009) already at the cloud base, high water vapour supersaturation up to 1% (Reutter et al., 2009) and high number concentration of aerosol particles freshly emitted by the fire up to $10^5\,cm^{-3}$ (Andreae et al., 2004; Reid et al., 2005) represent a particular setting for aerosol–cloud interactions. These clouds, known as pyrocumulus or pyrocumulonimbus (pyroCb) (Fromm et al., 2010), can occur anywhere in the world where there is sufficient fuel density to produce enough heat to trigger convection, but are most frequently observed in boreal forests (Nedelec et al., 2005; Rosenfeld et al., 2007) and tropical forests (Andreae et al., 2004). During the upward motion of the air due to the convective instability, the lifted condensation level is reached and a cumulus cloud starts to form. As shown by Luderer et al. (2006) a suitable background meteorology is the basic requirement for allowing the formation of deep pyroconvective clouds, which can even intersect the tropopause in extreme cases. Note that the sensible heat release by the fire is important to initialize the convection, but usually a fire cannot destabilize the complete overlaying troposphere. Therefore, the height of the pyroconvective cloud top depends strongly on the background meteorology.

In the last decade the study of pyroconvective clouds and their impact on weather and climate by transport of smoke and trace gases has attracted growing attention. For example, Fromm et al. (2000) showed an increase of tropospheric and stratospheric aerosol during the 1998 fire season in the Northern Hemisphere. The injection of tropospheric aerosol into the stratosphere was also shown in measurements and model simulations of the Chisholm pyrocumulonimbus of 2001 (Fromm and Servranckx, 2003; Trentmann et al., 2006; Rosenfeld et al., 2007; Fromm et al., 2008). An aerosol plume from an Australian fire was observed for several months well within the stratosphere (Fromm et al., 2006). For the Chisholm fire an extremely continental microphysical structure was documented (Rosenfeld et al., 2007). This means that the high aerosol concentration led to a high number of small cloud droplets, which led to an efficient suppression of precipitation formation within the updraft region. In a sensitivity study by Luderer et al. (2006) several conditions influencing pyroconvective clouds were varied, such as the sensible heat release by the fire, the aerosol concentration and the emission of water vapour by the fire. It was shown that the sensible heat release by the fire has the strongest effect on the development of the Chisholm pyrocumulonimbus, which is also consistent with other studies (Penner et al., 1986; Lavoué et al., 2000). When more sensible heat is available, the cloud reaches higher altitudes, thereby condensing and freezing more of the available water and releasing additional latent heat. The sensitivity simulations of the Chisholm pyrocloud on the aerosol concentration by Luderer et al. (2006) showed that the updraft region is only weakly affected by the aerosol loading, in contrast to the findings of other studies that had reported a stronger convection with increasing aerosol concentration (Andreae et al., 2004; Koren et al., 2005). It has to be noted that the study by Koren et al. (2005) investigated convective clouds over the ocean, which are not as vigorous as pyroconvective clouds. The reported invigoration of deep convection with increasing aerosol concentration has been explained by a delay in the formation of precipitation and the suppression of downdrafts and warm rain (Andreae et al., 2004; Koren et al., 2005; Rosenfeld et al., 2008). Therefore, more liquid condensate reaches higher altitudes, releasing more latent heat upon freezing. The additional latent heat release leads to an invigoration of the convection. Another aspect of cloud modification by aerosols concerns the cloud lifetime. Lindsey and Fromm (2008) showed that the highly polluted anvil of a pyroCb persisted 6–12 h longer than convectively generated cirrus anvils from clean convection in the vicinity of the pyroCb. Thus, pyroconvective clouds are a unique form of atmospheric convection in terms of microphysical and dynamical properties, which makes them an ideal test bed for investigations of aerosol–cloud interactions using high-resolution models. Using a broad set of different aerosol concentrations from very clean to very polluted, together with a fixed and intense dynamical trigger for cloud formation (sensible heat of the fire) offers the opportunity to attribute the differences in the simulations to the aerosol concentration.

In this study we focus on the influence of the aerosol number concentration on the microphysical structure and dynamical development of an idealized pyroconvective cloud. A crucial step in the microphysical evolution of a convective cloud is the activation of aerosol particles to form cloud droplets. The activation process affects the initial number and size of cloud droplets and can thus influence the progression of the convective cloud and the formation of precipitation. Although several studies in past years were able to reproduce the dynamical evolution of pyroconvective clouds well (Trentmann et al., 2006; Cunningham and Reeder, 2009), the activation of aerosol particles to cloud droplets was either neglected (Cunningham and Reeder, 2009) or parameterized in a strongly simplified way (Trentmann et al., 2006). In this study we improve the description of aerosol activation by the introduction of a look-up table specially computed for pyroconvective conditions using realistic aerosol size distributions and chemical properties (Reutter et al., 2009). This enables the microphysical scheme to simulate the aerosol activation in a more realistic way. For the first time, the interaction between microphysics and dynamics within a pyroconvective cloud can be studied in detail within a three-dimensional high-resolution model.

This paper is organized as follows: in the next section the ATHAM model and the set-up of the experiments are described. This is followed in Section 3 by the presentation and discussion of the results of sensitivity studies with three different aerosol concentrations.

2 Model description

The three-dimensional model ATHAM (Active Tracer High resolution Atmospheric Model) is able to simulate intense forms of atmospheric convection induced by volcanic eruptions or intense forest fires (Oberhuber et al., 1998; Graf et al., 1999; Textor et al., 2006; Tupper et al., 2009). The model solves the complete Navier–Stokes equations including sound waves, which cannot be excluded due to the possible supersonic flow around the vent of a volcano (Herzog et al., 2003). The model also contains the equation for tracer advection. The equations are solved with an implicit time-stepping scheme on a staggered Arakawa C grid (Arakawa and Lamb, 1977). This grid allows stretching for the use of a higher spatial resolution in regions where strong gradients can occur, e.g. in the vicinity of the fire. The dynamical core of ATHAM takes the effects of active tracers into account. An active tracer in this framework is defined as a component that affects the density, heat capacity, and compressibility of the air in the model. In this study, all hydrometeors and the smoke tracer are treated as active tracers. For the representation of sub-grid processes a prognostic turbulence scheme is implemented (Herzog et al., 2003), which allows

the differentiation between horizontal and vertical turbulent exchange processes when anisotropy in turbulence cannot be ignored.

For the calculation of microphysical processes within the pyroconvective clouds, in this study the two-moment mixed-phase bulk microphysical parameterization of Seifert and Beheng (2006) (SB scheme hereafter) has been implemented. It comprises the six hydrometeor categories of cloud water, rain water, cloud ice, snow, graupel and hail. For each category, mass and number densities are prognostic variables[1]. For a description of this scheme see also Blahak (2008) and Noppel et al. (2010). The information on the number and mass of the hydrometeors is essential for this study in order to simulate the aerosol–cloud interactions in pyroconvective clouds properly. For the activation of cloud droplets the SB scheme uses a look-up table that is not suitable for pyroconvective conditions. Therefore, a new look-up table was introduced, which is based on an aerosol activation study by Reutter et al. (2009). This study investigated the formation of cloud droplets under pyroconvective conditions using a parcel model that includes a detailed spectral description of cloud microphysics. It was found that the cloud droplet activation shows different dependencies on updraft velocity and aerosol concentration, depending on the ratio between the latter two variables. Hence, with the knowledge of the updraft velocity at the cloud base and the aerosol number concentration, the number of newly formed cloud droplets can be estimated through a look-up table. This table is characteristic for an aerosol size distribution with a median diameter of 120 nm, a geometric standard deviation of $\sigma_g = 1.5$ (Reid et al., 2005) and an effective hygroscopicity parameter of 0.2 (Petters and Kreidenweis, 2007; Andreae et al., 2008), which are typical values for young biomass burning aerosol. The required parameters for the look-up table are the updraft velocity w and the number of aerosol particles N_{CN}. Therefore, for each horizontal grid point the updraft velocity at the cloud base must be identified in the ATHAM simulation.

The cloud base in ATHAM is detected when the following criteria are fulfilled: (1) the updraft velocity w has to be larger than $0.1\,\mathrm{m\,s^{-1}}$, (2) the supersaturation S has to be larger than 0% and (3) the supersaturation at the next-lower model level has to be smaller than the supersaturation in the current model level. Most likely the updraft velocity at this location does not correspond exactly to a value in the look-up table, hence a linear interpolation is made between two tabulated values. In the model version used for this study, the look-up table has entries for nine different updraft velocities (1, 2.5, 5, 7, 10, 12, 15, 17 and 20 $\mathrm{m\,s^{-1}}$, see Table 1).

For the sensitivity studies regarding the aerosol particle concentration N_{CN}, a fixed value of N_{CN} is used for all grid points where the nucleation is calculated. The advantage of this method is that an exact number of N_{CN} can be prescribed, which is useful for idealized sensitivity studies. Note that N_{CN} in the model is only used for the activation of cloud droplets and therefore has no influence on other parameters. Also, the scavenging of aerosol particles by nucleation and impaction scavenging is not implemented in this version of ATHAM. Clearly, the scavenging of aerosol particles and hence the reduction of their number concentration is an important effect for the evolution of clouds and, in particular, for the vertical transport of aerosol particles through convective clouds. To improve the consistency between the sensitivity studies it is justified to neglect the reduction of the aerosol number concentration by scavenging. Nevertheless, in future studies, in particular when aerosol transport through pyroconvective clouds is assessed, the processes of nucleation and impaction scavenging should be included.

The model runs were initialized with a mid-latitude US standard atmosphere with no background wind. The model domain was set to $40\,\mathrm{km} \times 30\,\mathrm{km} \times 20\,\mathrm{km}$ with $110 \times 80 \times 55$ grid points in the x-y-z directions, respectively. The minimum horizontal and vertical grid box size was set to 50 m at the centre of the domain where the fire was located. Due to the stretched grid, the size of the grid boxes increases towards the borders of the model domain. The size of the fire front was set to $316\,\mathrm{m} \times 316\mathrm{m}$ and the energy release from the fire was calculated following Trentmann et al. (2006) with a fuel loading of $9\,\mathrm{kg\,m^{-2}}$, a rate of spread of $1.5\,\mathrm{m\,s^{-1}}$ and a value of $18700\,\mathrm{J\,kg^{-1}}$ for the standard heat of combustion (ASRD, 2001), which corresponds to a fire forcing of $252.45\,\mathrm{kW\,m^{-2}}$. Within the first minute of the simulation, the fire forcing is linearly increased from zero to the final fire forcing. After 60 min, the fire forcing is shut down linearly to zero within 1 minute. It should be noted that after switching off the fire forcing, the location of the fire is still warmer than the surroundings. Therefore, the updraft region still exists, but is very small compared to the conditions during the fire. For the smoke emissions, we used an emission factor of $9.1\,\mathrm{g\,kg_{fuel}^{-1}}$ (Andreae and Merlet, 2001). Note that the smoke released by the fire is not used as cloud condensation nuclei (CCN) but only as a tracer to illustrate the behaviour of the smoke plume. The time step was set automatically between 0.5 and 1.5 s in order to fulfil the Courant–Friedrichs–Levy criterion (Courant et al., 1928).

For the following studies, the aerosol number concentration for the activation of cloud droplets was set to three different cases: (i) a clean case with $N_{CN} = 200\,\mathrm{cm^{-3}}$, (ii) an intermediate case with $N_{CN} = 1000\,\mathrm{cm^{-3}}$ and (iii) a strongly polluted case with $N_{CN} = 20,000\,\mathrm{cm^{-3}}$. Note that the aerosol particle concentration of case (i) is very unrealistic for pyroconvective conditions. However, this case allows for the quantification of the effects that aerosol particles have on the evolution of pyroconvective clouds.

[1]The shape parameters of the Gamma distribution function for the cloud droplet size distribution are $\nu = \mu = 1$ (Seifert and Beheng, 2006)

Table 1. Number of cloud droplets in cm^{-3} for different cloud base updraft velocities w and initial aerosol concentration N_{CN} obtained from Reutter et al. (2009).

w, $m\,s^{-1}$	N_{CN}, cm^{-3}		
	200	1000	20 000
1.0	168.0	512.4	832.6
2.5	185.6	836.9	2922.0
5.0	188.4	914.6	7238.9
7.0	188.6	930.9	10 114.0
10.0	188.5	940.1	13 250.5
12.0	188.4	942.2	14 525.0
15.0	188.4	942.9	15 933.8
17.0	188.3	943.0	16 478.9
20.0	188.2	942.9	17 212.9

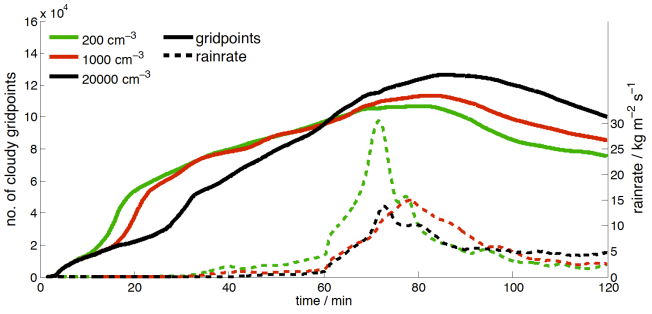

Figure 1. Temporal evolution of (solid lines) the number of cloudy grid points for aerosol concentrations of (green) $N_{CN} = 200\,cm^{-3}$, (red) $N_{CN} = 1000\,cm^{-3}$ and (black) $N_{CN} = 20000\,cm^{-3}$ as well as (dashed) for the rain rate in $kg\,m^{-2}\,s^{-1}$ of the three specified aerosol concentrations.

3 Results

The aim of this study is to investigate the sensitivity of the microphysical and dynamical structure of a pyroconvective cloud on aerosol concentrations representing clean, intermediate and strongly polluted conditions. First, we analyse the dynamical evolution and the transport of smoke. After that, the microphysical differences between the different aerosol conditions are investigated.

3.1 Dynamical evolution

Figure 1 shows the temporal evolution of the number of cloudy grid points, which is a measure for the size or volume of the pyroclouds for the different aerosol particle concentrations. A grid point is identified as cloudy as soon as one hydrometeor category shows a water content larger than $3 \times 10^{-7}\,g\,kg^{-1}$. The results show the most rapid development in terms of size for the clean case, while the strongly polluted case is characterized by a comparatively slow evolution. After 60 min, all three pyroclouds show approximately the same number of cloudy grid points. At this time, the fire is shut down and thereby the external forcing that drives convection is removed. No clear signal of the shutdown of the fire is visible in the size of the clouds. On the right axis, the rain rates for all cases show a significant increase shortly after the fire is shut down. However, the maximum cloud size, and the time when this maximum is reached, differ for all three cases. The maximum number of cloudy grid points reached during 2 hours of simulation is smallest for the clean case (106 858) after 79.5 min. In the intermediate case the maximum of 113 357 cloudy grid points is reached after 84.1 min, while the strongly polluted case reaches its maximum (126 682 cloudy grid points) 1 minute later (85.3 min). This means that with increasing aerosol concentration the maximum size of the cloud also increases and the maximum occurs later. Note, due to the stretched grid, the number of cloudy grid points is not directly proportional to the cloud size. However, especially in the first half of the simulation, the number of cloudy grid points is an appropriate measure to quantify the influence of aerosol particles on the dynamical evolution of pyroconvective clouds. After reaching the maximum size, all three clouds decay at a comparable speed. In contrast, the rain rate is largest for the clean case after 71.7 min of the simulation and smallest for the strongly polluted case. In this study, precipitation reaching the surface is used to calculate the rain rate. This indicates that the dynamical evolution of a strongly polluted pyroconvective cloud is limited in the beginning, but more sustainable, pointing to a cloud lifetime effect resulting from the higher aerosol loading and the reduced precipitation (Lohmann and Feichter, 2005).

Interestingly, from a dynamical point of view, the clean and intermediate polluted cases show a very similar behaviour. The only noteworthy differences are that the clean case shows an earlier onset of the rapid evolution (~ 5 min) and reaches the maximum size earlier than the intermediate polluted case. The rapid evolution is triggered by the latent heat release, when large amounts of cloud and rain droplets freeze and form ice crystals, snow and graupel. This is supported by the temporal evolution of the average water content of each hydrometeor (Fig. 3 in Sect. 3.2). The additional latent heat results in a higher updraft velocity and hence in a more rapid growth of the pyroconvective cloud (Rosenfeld et al., 2008). However, a different pattern is seen for the precipitation rate in Fig. 1. Here, the intermediate and strongly polluted case show similar behaviour, and both have a significantly reduced ($\sim$ factor of 2) rain rate compared to the clean case. This will be examined in detail in Section 3.2.

Another measure for the dynamical evolution of a pyroconvective cloud is the vertical distribution of the smoke tracer. Figure 2 shows the averaged vertical distribution for the three cases after 30, 60 and 90 min, respectively. Note that the different aerosol concentrations are only used for the activation of the cloud droplets and have no influence on the smoke tracer that is emitted by the fire. Therefore, the emitted smoke tracer by the fire is equal for all three cases

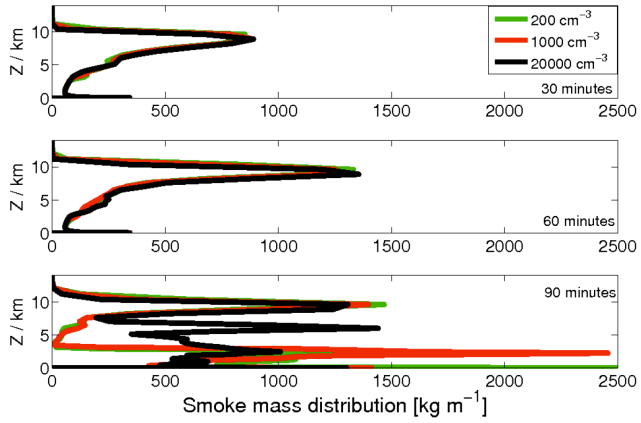

Figure 2. Averaged vertical distribution of smoke mass per unit length altitude for (green) $N_{CN} = 200\,cm^{-3}$, (red) $N_{CN} = 1000\,cm^{-3}$ and (black) $N_{CN} = 20\,000\,cm^{-3}$ after 30, 60, and 90 min of simulation, respectively.

and indicates the structure of the smoke plume. After 30 min the height of the maximum of the smoke mass distribution (h_{smoke}) is highest for the cleanest case ($h_{smoke} = 9600$ m), followed by the two polluted cases ($h_{smoke} = 8900$ m). After 60 min the amount of smoke mass at h_{smoke} increases similarly for all cases, while h_{smoke} increases for the intermediate case to 9600 m and stays constant for the other two cases. Ninety minutes after ignition of the fire the vertical smoke mass distribution shows a complex structure. This is due to the decay of the cloud after the shutdown of the fire 60 min after ignition. There is still a local maximum at a height of 10 km. However, the strong updraft from the fire is now missing and the smoke tracer is sedimenting out. In the very polluted case, a local maximum of the smoke mass concentration is present at about 5 km. This is due to the fact that the cloud in the strongly polluted case reaches its maximum last. Therefore, the sedimentation of the smoke mass is also delayed. Nevertheless, these results show that the aerosol concentration only weakly affects the cloud top height.

3.2 Microphysical evolution

The temporal evolution of the total liquid and frozen water content (in g kg^{-1}) averaged over the complete model domain is shown in Fig. 3 in order to investigate the differences in the microphysics due to the differing aerosol loadings. It can be seen that the appearance for the six hydrometeor classes (cloud droplets, rain, ice particles, snow, graupel, and hail) is different for the three cases. In all cases, the formation of rain droplets is the first process after the activation of cloud droplets. In the clean case, this is followed by the production of ice crystals, snow, and graupel, respectively. The last hydrometeor class to appear is hail. During the first hour of the simulation, the hydrometeor class with the largest average water content is graupel. After 65 min, 5 min after the fire

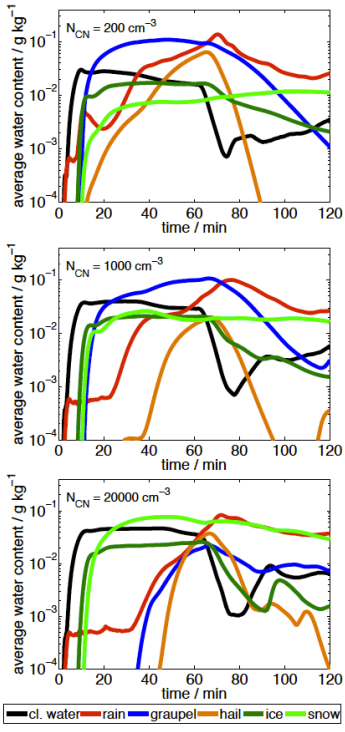

Figure 3. Temporal evolution of the averaged water content [g kg^{-1}] in the model domain for the six hydrometeor classes (black) cloud water, (red) rain water, (dark green) ice, (light green) snow, (blue) graupel and (orange) hail for (top) the clean case with $N_{CN} = 200\,cm^{-3}$, (middle) the intermediate case with $N_{CN} = 1000\,cm^{-3}$ and (bottom) the strongly polluted case with $N_{CN} = 20\,000\,cm^{-3}$.

is completely turned off, the production of cloud droplets is strongly reduced due to the drastically reduced updraft at the cloud base and the average water content of cloud droplets decreases strongly. Also, the mass concentration of the hail particles decreases due to the reduced growth of the hail particles through riming of cloud droplets. Therefore, the production and growth of new hail is suppressed after the fire is turned off. At the end of the simulation after 120 min, rain and snow are the dominant hydrometeor classes regarding the water mass within the pyroconvective cloud, while hail has been completely removed from the atmosphere by sedimentation.

In the intermediate case ($N_{CN} = 1000\,cm^{-3}$) the activation of cloud droplets is also followed by the formation of rain droplets. However, after an initial production phase, the rain droplet formation stagnates for about 20 min and only afterwards are rain droplets produced in a significant amount. After the initial production of rain, ice crystals develop, followed by snow and graupel, respectively. Again, hail is the last hydrometeor class to appear. After the shutdown of the fire in the intermediate case, rain and graupel are the dominant hydrometeors. Again, as in the clean case, cloud droplets and hail show the fastest response to the shutdown

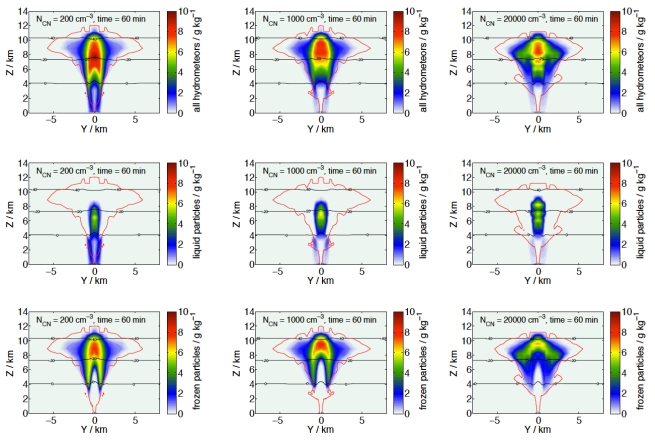

Figure 4. Y–Z cross section at $x = 0$ km of (top row) the total hydrometeor water content in g kg^{-1}, (middle row) the liquid water content in g kg^{-1} and (bottom row) the frozen water content in g kg^{-1} after 60 min simulation time for (left) $N_{CN} = 200\,cm^{-3}$, (middle) $N_{CN} = 1000\,cm^{-3}$ and (right) $N_{CN} = 20000\,cm^{-3}$. The black lines denote the 0 °C, 0–20 °C and −40 °C isotherms, respectively. The red line shows the 0.1 µg kg^{-1} isoline of the interstitial aerosol, which describes the shape of the smoke plume.

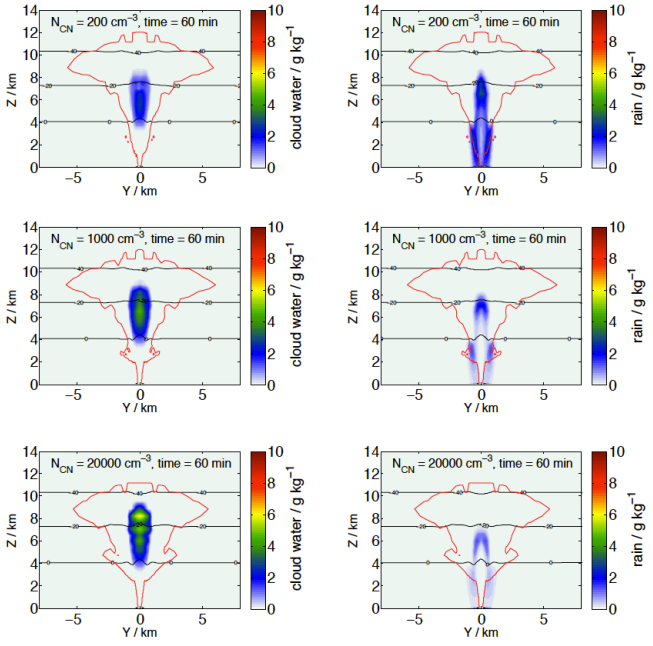

Figure 5. Y–Z cross section at $x = 0$ km of the (left column) cloud water content in g kg^{-1} and (right column) rain water content in g kg^{-1} for (top row) the clean case, (middle row) the intermediate case and (bottom row) the strongly polluted case. The black lines denote the 0 °C, 0–20 °C and −40 °C isotherms, respectively. The red line shows the 0.1 µg kg^{-1} isoline of the interstitial aerosol.

of the fire. Also, all other hydrometeors start to decrease in terms of average water content except for the rain, which increases due to the falling and then melting graupel and hail particles. After 120 min, rain and snow are the most abundant hydrometeors.

In the strongly polluted case the formation of significant amounts of rain, graupel and hail is clearly delayed and separated from the formation of ice crystals and snow, which is the dominant hydrometeor almost throughout the complete simulation time. After the shutdown of the fire only rain and snow exist in a significant amount. The other hydrometeors decrease due to the missing updraft from the fire. The falling graupel and hail particles are partly melting, which results in an increase of rain droplets. Interestingly, when snow is produced in the beginning, its averaged water content throughout the simulations stays at a constant level for all three cases.

In Fig. 4, the y–z cross sections at $x = 0$ km of the three different pyroconvective clouds after 60 min show the water content in g kg^{-1} and the 0.1 µg kg^{-1} isoline of the interstitial aerosol, describing the shape of the smoke plume for (top row) all hydrometeors, (middle row) the liquid phase and (bottom row) the frozen phase. The results show that, even under vigorous dynamical forcing by the fire, the aerosol concentration has an influence on the distribution of water within the cloud and also on the precipitation. The maximum of the total hydrometeor content can be found in the clean case, where in the updraft region values of up to 9.5 g kg^{-1} are visible. Also in this case the most pronounced precipitation pattern of all three cases can be observed, even within the updraft region of the cloud, which indicates large rain droplets. With increasing aerosol concentration, the maximum hydrometeor content and the amount of precipitation decreases, while the hydrometeor content in the outer regions of the cloud is significantly increased. The middle row of Fig. 4 also shows that the supercooled liquid particles (cloud and rain droplets) reach a maximum altitude of about 8600 m for the clean case and about 9500 m for the strongly polluted case. It can also be seen that the precipitation reaching the ground consists purely of rain droplets. Note that this rain is mainly formed by precipitating graupel and hail particles, which melt to rain droplets after they cross the 0 °C isoline. It should be noted that these figures are snapshots of time-dependent variables after 60 min of the model run. However, this is the time where the pyroCb shows a more or less equilibrium state for the microphysical properties, which is confirmed by simulations without the shutdown of the fire (not shown). To understand the distribution of the liquid and frozen water, the composition of the cloud is discussed in more detail for each case in the following.

Figure 5 shows a y–z cross section of the cloud and rain water content for each case. Here it can be clearly seen that the cloud water content is increasing with increasing aerosol pollution, while the rain water content shows the opposite effect, which can be explained by the number and size of the cloud droplets. For the clean case, the cloud droplet number is low and therefore the mean volume radius of the cloud droplets is large (up to 20 µm, see Supplement), which allows

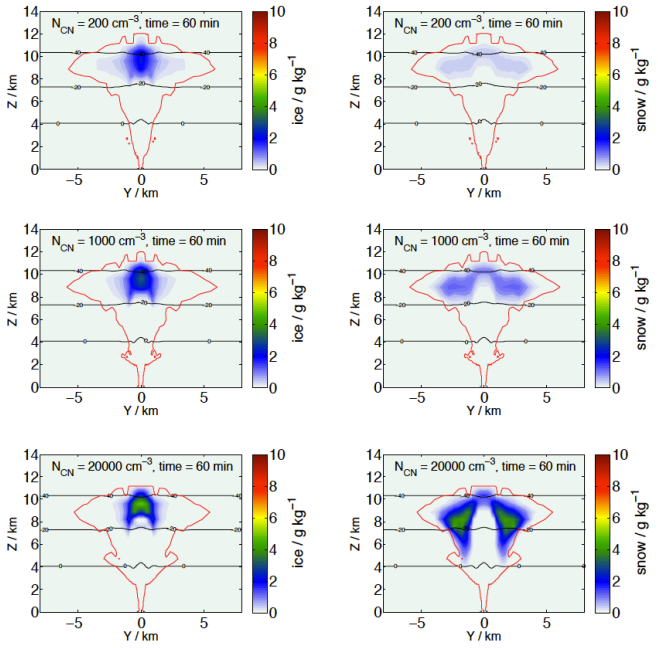

Figure 6. Y–Z cross section at $x = 0$ km of the (left column) ice water content in g kg^{-1} and (right column) snow water content in g kg^{-1} for (top row) the clean case, (middle row) the intermediate case and (bottom row) the strongly polluted case. The black lines denote the 0 °C, 0–20 °C and −40 °C isotherms, respectively. The red line shows the 0.1 µg kg^{-1} isoline of the interstitial aerosol.

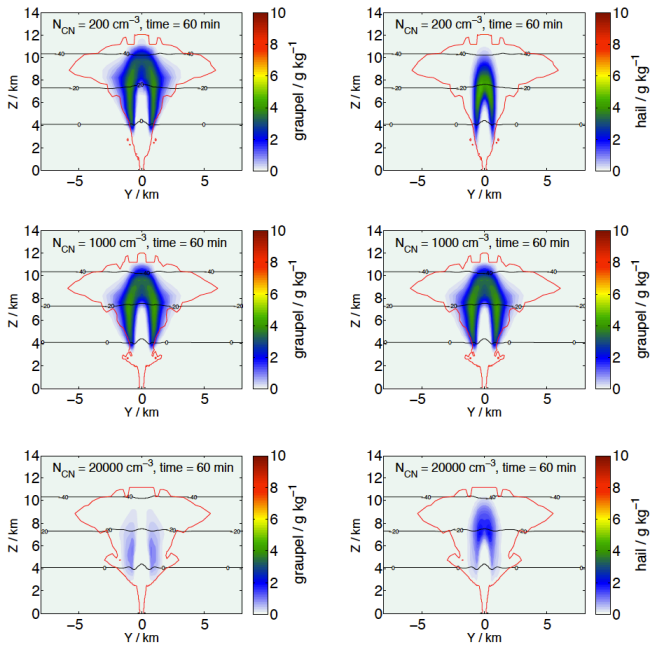

Figure 7. Y–Z cross section at $x = 0$ km of the (left column) graupel water content in g kg^{-1} and (right column) hail water content in g kg^{-1} for (top row) the clean case, (middle row) the intermediate case and (bottom row) the strongly polluted case. The black lines denote the 0 °C, 0–20 °C and −40 °C isotherms, respectively. The red line shows the 0.1 µg kg^{-1} isoline of the interstitial aerosol.

a fast transition to rain droplets by autoconversion and accretion. Note that in the clean case an important part of the rain formation also occurs by melting of large frozen particles (hail and graupel), which can be seen by the outer bands of precipitation at $y = \pm 0.5$ km in Fig. 5. Nevertheless, in order to form graupel and especially hail, a sufficient amount of rain droplets is crucial. Therefore, the earliest and strongest onset of precipitation is due to the large rain droplets and their influence on the larger frozen hydrometeors in the clean case.

In the intermediate case, the cloud water content is already significantly larger and much less rain water is present. The larger amounts of CCN particles lead to more but smaller cloud droplets and therefore the efficiency of autoconversion and accretion is reduced, which leads to a reduction of rain water. In the strongly polluted case, the cloud droplets are extremely small (mean volume radius < 6 µm), which leads to an inefficient production of rain droplets by autoconversion or accretion.

Figure 6 shows the cross section of the cloud ice and snow water content for the three different aerosol concentrations. Again, large differences between the different aerosol loadings can be observed, with the smallest amount of cloud ice and snow for the clean case. This is consistent with the results for the liquid particles, because in this case the freezing of cloud droplets forms cloud ice. In the next step, snow is formed by aggregation of cloud ice. Due to the lower amount of cloud droplets in the clean case and hence the lower amount of cloud ice, only a small amount of snow is produced. When the aerosol concentration is increased, the cloud droplet concentration is also increased and therefore more cloud droplets are transported to heights where they freeze and form cloud ice. This enhanced production of ice crystals also leads to a higher production of snow. In the strongly polluted case the snow class is the most abundant particle class during the first hour of the simulation, and is spread all across the supercooled regions of the cloud, except in the vigorous updraft region.

Figure 7 shows the water content of the two largest frozen hydrometeor classes, graupel and hail. The clean case shows the largest amounts of graupel and hail, which can be found even at heights where the temperature is above the freezing point of water. In this region graupel and hail melt and are transferred to the rain class. It can also be seen that the graupel particles are more horizontally spread than the hail particles, which can be explained by their size. The smaller graupel particles with a mean volume radius of up to 900 µm in the upper regions of the cloud can be transported horizontally before they start to sediment. The hail particles are already so large in the upper parts of the cloud that they start to fall down before they can be transported to the outer regions of the cloud. In the intermediate case, the amount

of hail is significantly reduced compared to the clean case, while the amount of graupel is only slightly reduced. The hail formation in the intermediate case is suppressed by the delayed production of rain droplets, although the formation of graupel is similar for the clean and intermediate case. In the strongly polluted case, the hail water content after 60 min is very similar compared to the results of the intermediate case. However, the graupel water content in the strongly polluted case is drastically reduced compared to the other two cases. The reason for this is that the deposition to snow is much more efficient than the formation and riming of graupel. The sizes of the graupel particles in the strongly polluted case are the largest of all three cases, with a mean volume radius of up to 1.6 mm, while in the other two cases the largest graupel particles have a mean volume radius of 1 to 1.4 mm. Therefore, the graupel particles in the strongly polluted case start to precipitate and are transferred into the rain class as soon as they reach an altitude with a temperature above 0° C. The production of hail in the strongly polluted case goes alongside the rain formation, which shows behaviour comparable to the intermediate case. Therefore, the amount of hail in both cases is comparable.

From the investigations of the dynamical and microphysical properties of the three different cases presented above, the following conclusions can be drawn. After the rapid formation of rain by autoconversion of cloud droplets in the clean case, graupel and hail are formed within a short period of time. This means that at an early stage of the cloud evolution a significant amount of water is already transferred to the frozen phase. This leads to a strong release of latent heat due to the phase transition, resulting in a rapid evolution of the cloud (Fig. 1, green line around 10 min). On the other hand, the rain droplets, graupel and hail particles grow rapidly and soon start to precipitate, beginning 28 min after model start. After the shut down of the fire the dominant updraft is missing and all large hydrometeors, especially graupel and hail, fall out of the cloud, leading to a strongly enhanced rain rate. In the decaying phase, rain and snow are the dominant hydrometeors.

In the intermediate case, the formation of rain is slower compared to the clean case, because the cloud droplets are smaller. Therefore, the formation of ice crystals and snowflakes triggers the formation of graupel, and hence the freezing of large amounts of water by freezing rain droplets is delayed in this case. Therefore, the rapid evolution of the intermediate polluted cloud is shifted to a later time (16 min). Because the formation of hail depends on the freezing of large rain droplets, the evolution of hail is also delayed. However, the precipitation starts almost at the same time compared to the clean case. After the shutdown of the fire the rain rate also increases, but is only half as strong as in the clean case, because more water stays in the cloud, especially in the snow class.

In the strongly polluted case, the formation of rain, graupel and hail is even more delayed compared to the previous cases, because of the very small size of the cloud droplets. This leads to a delay in the freezing of larger amounts of water in the cloud, and hence the rapid increase in the size of the cloud is postponed until sufficient amounts of cloud and rain droplets are available for freezing (20 min). Additionally, the onset of precipitation is the latest of all the three cases and begins only after 40 min. The cloud in the strongly polluted case, which is the largest in size, shows similar behaviour as the intermediate case after the fire is turned off. Coincidentally, after 1 hour of simulation, all clouds show approximately the same size.

The shapes of the interstitial aerosol plumes for each case (red contour lines in Figs. 5 to 7) show differences on small scales after 60 min, in addition to the differing vertical distribution of the aerosol mass (Fig. 2). The interstitial aerosol plume is rather narrow below an altitude of 7 km for the clean and intermediate cases. In contrast, in the strongly polluted case it is broader between 4 and 6 km. However, the horizontal extension of the interstitial aerosol plume at an altitude of 9 km is slightly larger for the clean and intermediate cases than in the strongly polluted case. Note that these isolines denote only the shape of the smoke plume. In terms of the vertical distribution of the aerosol mass, the differences between the three cases are very small. Therefore, whereas the aerosol concentration has a rather small influence on the size of a mature pyroconvective cloud, is very important for its microphysical evolution. A key point is the shift in the onset and amount of precipitation with increasing aerosol concentration.

After the shutdown of the fire in the model (60 min after model start) the response in the simulated number of cloudy grid points is rather slow. However, it is clearly visible that the rain rate increases strongly after the shutdown of the fire. The strongest signal is exhibited by the clean case, because here the largest hydrometeors occur. Due to the termination of the strong sensible heat release by the fire, the main buoyancy source for the updraft is lacking, and therefore the larger hydrometeor classes (rain, graupel and hail) start to precipitate. The frozen particles then melt at higher temperatures and are converted into rain.

The rain rates for the intermediate and strongly polluted cases are reduced due to the large amount of smaller frozen hydrometeors, which either sublimate (ice crystals) or start to sediment slowly (snowflakes) due to the missing updraft. Therefore, the number of cloudy grid points is reduced first for the clean case. The largest cloud extension after 120 min is visible for the strongly polluted case. This is in agreement with cloud lifetime effect, which says that smaller cloud droplets decrease the precipitation efficiency and hence prolong the cloud lifetime (Lohmann and Feichter, 2005). Note that in this model set-up we do not take radiative effects into account. However, due to the different microphysical properties of the different cases, a significant change of the radiative effects can be expected (cloud albedo effect).

The emitted smoke and its influence on the microphysical structure and the subsequent radiative effects can have significant consequences on a larger scale. Although a complete climatology for intense pyroCbs is not available, the year 2002 showed at least 17 pyroCbs in North America, which reached the tropopause layer (Fromm et al., 2010). The Large Fire Database (Stocks et al., 2003) contains more than 10 000 large fires from 1959 to 1997 in Canada, each with the potential for pyroCb formation. Therefore, one can assume that pyroCbs are a frequent phenomenon in temperate and boreal regions, with an even higher occurrence of weaker pyrocumulus clouds. This shows that pyroclouds need to be considered when investigating the influence of clouds and aerosol on climate.

4 Summary and discussion

In this study the influence of the aerosol concentration on the dynamical and microphysical evolution of a pyroconvective cloud has been investigated. The main achievements and findings of the study are that

- a first investigation has been presented of the influence of aerosol particles on the evolution of a pyroCb using a realistic description of the activation of cloud droplets and realistic aerosol number concentrations
- clear and distinct differences in the microphysical evolution of a pyrocumulonimbus cloud are found depending on the aerosol concentration
- no clear influence of aerosol particles on the dynamical evolution and the smoke transport has been found.

In the following, the main methodology and results are summarized and discussed. To investigate the aerosol–pyroCb interaction, a sophisticated two-moment microphysical scheme (Seifert and Beheng, 2006) has been implemented into the cloud-resolving model ATHAM. To study the influence of different aerosol concentrations on pyroconvective clouds, a look-up table based on the results of a cloud droplet activation study (Reutter et al., 2009) was included into the microphysical scheme.

Sensitivity studies have been conducted with three different aerosol concentrations: (i) a clean case with an aerosol concentration of $N_{\mathrm{CN}} = 200\,\mathrm{cm}^{-3}$, (ii) an intermediate case with $N_{\mathrm{CN}} = 1000\,\mathrm{cm}^{-3}$ and (iii) a strongly polluted case with $N_{\mathrm{CN}} = 20,000\,\mathrm{cm}^{-3}$, which is a typical value for pyroconvective clouds (Reid et al., 2005). After 60 min of model integration, the influence of the aerosol concentration on the dynamical evolution of the pyroconvective cloud is rather weak in terms of the size of the cloud and the smoke distribution within the cloud. In contrast, the aerosol concentration has a strong impact on the microphysical evolution of pyroconvective clouds despite the strong dynamical forcing by the fire.

In the clean case, rain forms rapidly by autoconversion of cloud droplets. Due to the low number concentrations of aerosol particles and the high supersaturation produced by the strong updraft in the pyroconvective cloud, the cloud droplets are large and hence the autoconversion is an efficient process for rain formation. Shortly after, ice crystals, snow, and graupel are formed within a short period of time. Hence, at an early stage of the cloud life cycle a significant amount of water is already transferred to the frozen phase, which leads to an additional release of latent heat that further intensifies the strong updraft region. The rain droplets, hail and graupel particles grow fast and soon start to precipitate.

In the intermediate aerosol case, the formation of rain is slower compared to the clean case. This is due to the fact that the higher aerosol concentration leads to more but smaller cloud droplets, which reduces the efficiency of the autoconversion. Therefore, the formation of ice crystals and snowflakes becomes more important for the eventual formation of graupel and hail. Compared to the clean case, the freezing of water and hence the rapid growth of the cloud is delayed.

In the strongly polluted case, the formation of rain, graupel and hail is even more delayed compared to the previous cases, because of the extremely small cloud droplets in this case. In the beginning of the simulation only cloud droplets, ice crystals and snowflakes can be formed, which leads to the latest formation of precipitation in all three cases.

Overall, after 1 hour, all three cases show the same size of the pyroconvective cloud. At this point, the fire forcing in the model is switched off. Soon after that the rain rate in all three cases increases, because all large hydrometeors in the cloud are sedimenting out due to the missing fire-induced updraft. However, for the intermediate and strongly polluted case the rain rate is significantly smaller compared to the clean case. On the other hand, the maximum size of the cloud is increased when the aerosol concentration is increased. Also, the time of the maximum size occurs later in the more polluted cases (cloud lifetime effect).

Overall it can be concluded that the microphysical structure of a pyroconvective cloud is very sensitive to the aerosol concentration in the range between $N_{\mathrm{CN}} = 200\,\mathrm{cm}^{-3}$ and $N_{\mathrm{CN}} = 20,000\,\mathrm{cm}^{-3}$ in the rising plume, which leads to a delay of precipitation with increasing pollution.

Various studies have shown a different microphysical evolution of clouds for different aerosol concentrations in observational data (Costa et al., 2000; Andreae et al., 2004) and in model simulations (Khain et al., 2005; Seifert and Beheng, 2006; Diehl et al., 2007; Tao et al., 2007; Storer and van den Heever, 2013), which are consistent with the findings of this study. However, in most 3-D model simulations (Khain et al., 2005; Seifert and Beheng, 2006; Tao et al., 2007; Seifert et al., 2012) the sensitivity of the aerosol concentration on the evolution of clouds was studied in the range between $N_{\mathrm{CN}} = 100\,\mathrm{cm}^{-3}$ and $N_{\mathrm{CN}} = 3200\,\mathrm{cm}^{-3}$, assuming a model salt that is like the very hydrophilic sodium

chloride ($\kappa = 1.28$). This is very unrealistic for pyroconvective clouds, because during a biomass-burning event a high number of less hydrophilic particles ($\kappa < 0.6$) are emitted. Admittedly, the sensitivity on the aerosol concentration is larger when more hydrophilic particles like sodium chloride are used. Therefore, the cloud evolution is similar for set-ups with lower aerosol concentration but higher hygroscopicity, and with higher aerosol concentration but lower hygroscopicity (as considered in this study). Storer and van den Heever (2013) conducted model simulations with a similar approach of CCN activation, using a look-up table obtained by parcel model simulations. However, they focused on tropical deep convection, which is influenced by aerosol concentrations up to $3200\,\mathrm{cm}^{-3}$.

For the first time, the impact of the aerosol concentration on the evolution of a pyroconvective cloud has been studied here with a realistic description of the activation of cloud droplets from very clean to strongly polluted conditions using activation properties corresponding to freshly emitted biomass burning aerosol. However, more studies are needed to further improve our understanding of the influence of aerosol concentration on the evolution of pyroconvective clouds, using realistic meteorological conditions to comprise also effects such as background winds or more realistic atmospheric profiles of temperature and humidity.

The Supplement related to this article is available online at doi:10.5194/acp-14-7573-2014-supplement.

Acknowledgements. This work has been supported by an International Max Planck Research School fellowship and the Max Planck Society. The authors would like to thank M. Fromm and one anonymous reviewer for very helpful questions and comments. P. Reutter thanks M. Voigt and F. Gierth for technical support, P. Spichtinger for helpful discussions and B. Dylan for inspiration.

The service charges for this open access publication have been covered by the Max Planck Society.

Edited by: P. Stier

References

Andreae, M. O. and Merlet, P.: Emission of trace gases and aerosols from biomass burning, Global Biogeochem. Cy., 15, 955–966, 2001.

Andreae, M. O. and Rosenfeld, D.: Aerosol-cloud-precipitation interactions. Part 1: The nature and sources of cloud-active aerosols, Earth Sci. Rev., 89, 13–41, doi:10.1016/j.earscirev.2008.03.001, 2008.

Andreae, M. O., Rosenfeld, D., Artaxo, P., Costa, A. A., Frank, G. P., Longo, K. M., and Silva-Dias, M. A. F.: Smoking rain clouds over the Amazon, Science, 303, 1337, doi:10.1126/science.1092779, 2004.

Arakawa, A. and Lamb, V. R.: Computational design of the basic dynamical processes of the ucla general circulation model, in: General Circulation Models of the Atmosphere, Academic Press, New York, 173–265, 1977.

ASRD: Final Documentation Report – Chisholm Fire (LWF-063), Forest Protection Division, ISBN 0-7785-1841-8, Tech. rep., Alberta Sustainable Resource Development, 2001.

Blahak, U.: Towards a better representation of high density ice particles in a state-of-the-art two-moment bulk microphysical scheme, in: Proc. 15th Int. Conf. Clouds and Precip., Cancun, Mexico, 2008.

Costa, A. A., de Oliveira, C. J., de Oliveira, J. C. P., and da Costa Sampaio, A. J.: Microphysical observation of warm cumulus clouds in Ceara, Brazil, Atmos. Res., 54, 167–199, 2000.

Courant, R., Friedrichs, K., and Lewy, H.: Über die partiellen Differenzengleichungen der mathematischen Physik, Mathematische Annalen, 100, 32–74, 1928.

Cunningham, P. and Reeder, M. J.: Severe convective storms initiated by intense wildfires: Numerical simulations of pyro-convection and pyro-tornadogenesis, Geophys. Res. Lett., 36, L12812, doi:10.1029/2009GL039262, 2009.

Diehl, K., Simmel, M., and Wurzler, S.: Effects of drop freezing on microphysics of an ascending parcel under biomass burning conditions, Atmos. Environ., 41, 303–314, 2007.

Fromm. M. and Servranckx. R.: Transport of forest fire smoke above the tropopause by supercell convection, Geophys. Res. Lett., 30, 142, doi:10.1029/2002GL016820, 2003.

Fromm, M., Alfred, J., Hoppel, K., Hornstein, J., Bevilacqua, R., Shettle, E., Servranckx, R., Li, Z., and Stocks, B.: Observations of boreal forest fire smoke in the stratosphere by POAM III, SAGE II, and lidar in 1998, Geophys. Res. Lett., 27, 1407–1410, 2000.

Fromm, M., Tupper, A., Rosenfeld, D., Servranckx, R., and McRae, R.: Violent pyro-convective storm devastates Australia's capital and pollutes the stratosphere, Geophys. Res. Let, 33, L05815, doi:10.1029/2005GL025161, 2006.

Fromm, M., Torres, O., Diner, D., Lindsey, D., Vant Hull,B., Servranckx, R., Shettle, E .P., and Li, Z.: Stratospheric impact of the Chisholm pyrocumulonimbus eruption: 1. Earth-viewing satellite perspective, J. Geophys. Res., 113, D08202, doi:10.1029/2207JD009153, 2008.

Fromm, M., Lindsey, D. T., Servranckx, R., Yue, G., Trickl, T., Sica, R., Doucet, P., and Godin-Beekmann, S.: The untold story of pyrocumulonimbus, B. Am. Meteorol. Soc., 91, 9, 1193–1209, doi:10.1175/2010BAMS3004.1, 2010.

Graf, H.-F., Herzog, M., Oberhuber, J. M., and Textor, C.: The effect of environmental conditions on volcanic plume rise, J. Geophys. Res., 104, 24309–24320, 1999.

Herzog, M., Graf, H.-F., and Oberhuber, J. M.: A prognostic turbulence scheme for the nonhydrostatic plume model ATHAM, J. Atmos. Sci., 60, 2783–2796, 2003.

Khain, A., Rosenfeld, D., and Pokrovsky, A.: Aerosol impact on the dynamics and microphysics of deep convective clouds, Q. J. Roy. Meteorol. Soc., 131, 2639–2663, 2005.

Koren, I., Kaufman, Y. J., Rosenfeld, D., Remer, L. A., and Rudich, Y.: Aerosol invigoration and restructuring of Atlantic convective clouds, Geophys. Res. Lett., 32, L14828, doi:10.1029/2005GL023187, 2005.

Lavoué, D., Liousse, C., Cachier, H., Stocks, B. J., and Goldammer, J. G.: Modeling of carbonaceous particles emitted by boreal and temperate wildfires at northern latitudes, J. Geophys. Res., 105, 26871–26890, 2000.

Lindsey, D. T. and Fromm, M.: Evidence of the cloud lifetime effect from wildfire-induced thunderstorms, Geophys. Res. Lett., 35, L22809, doi:10.1029/2008GL035680, 2008.

Lohmann, U. and Feichter, J.: Global indirect aerosol effects: a review, Atmos. Chem. Phys., 5, 715–737, doi:10.5194/acp-5-715-2005, 2005.

Luderer, G., Trentmann, J., Winterrath, T., Textor, C., Herzog, M., Graf, H. F., and Andreae, M. O.: Modeling of biomass smoke injection into the lower stratosphere by a large forest fire (Part II): sensitivity studies, Atmos. Chem. Phys., 6, 5261–5277, doi:10.5194/acp-6-5261-2006, 2006.

Nedelec, P., Thouret, V., Brioude, J., Sauvage, B., Cammas, J.-P., and Stohl, A.: Extreme CO concentrations in the upper troposphere over northeast Asia in June 2003 from the in situ MOZAIC aircraft data, Geophys. Res. Lett., 32, L14807, doi:10.1029/2005GL023141, 2005.

Noppel, H., Blahak, U., Seifert, A., and Beheng, K. D.: Simulations of a hailstorm and the impact of CCN using an advanced two-moment cloud microphysical scheme, Atmos. Res., 96, 286–301, 2010.

Oberhuber, J., Herzog, M., Graf, H.-F., and Schwanke, K.: Volcanic plume simulation on large scales, J. Volcanol. Geoth. Res., 87, 29–53, 1998.

Penner, J. E., Haselman, Jr., L. C., and Edwards, L. L.: Smoke-plume distribution above large-scale fires: implications for simulations of "nuclear winter", J. Clim. Appl. Meteorol., 25, 1434–1444, 1986.

Petters, M. D. and Kreidenweis, S. M.: A single parameter representation of hygroscopic growth and cloud condensation nucleus activity, Atmos. Chem. Phys., 7, 1961–1971, doi:10.5194/acp-7-1961-2007, 2007.

Reid, J. S., Koppmann, R., Eck, T. F., and Eleuterio, D. P.: A review of biomass burning emissions part II: intensive physical properties of biomass burning particles, Atmos. Chem. Phys., 5, 799–825, doi:10.5194/acp-5-799-2005, 2005.

Reutter, P., Su, H., Trentmann, J., Simmel, M., Rose, D., Gunthe, S. S. Wernli, H., Andreae, M. O., and Pöschl, U.: Aerosol- and updraft-limited regimes of cloud droplet formation: influence of particle number, size and hygroscopicity on the activation of cloud condensation nuclei (CCN), Atmos. Chem. Phys., 9, 7067–7080, doi:10.5194/acp-9-7067-2009, 2009.

Rosenfeld, D., Fromm, M., Trentmann, J., Luderer, G., Andreae, M. O., and Servranckx, R.: The Chisholm firestorm: observed microstructure, precipitation and lightning activity of a pyro-cumulonimbus, Atmos. Chem. Phys., 7, 645–659, doi:10.5194/acp-7-645-2007, 2007.

Rosenfeld, D., Lohmann, U., Raga, G. B., O'Dowd, C. D., Kulmala, M., Fuzzi, S., Reissell, A., and Andreae, M. O.: Flood or drought: how do aerosols affect precipitation?, Science, 321, 1309–1313, 2008.

Seifert, A. and Beheng, K.: A two-moment cloud microphysics parameterization for mixed-phase clouds. Part II: Deep convective storms, Meterol. Atmos. Phys., 92, 67–88, 2006.

Seifert, A., Köhler, C., and Beheng, K. D.: Aerosol-cloud-precipitation effects over Germany as simulated by a convective-scale numerical weather prediction model, Atmos. Chem. Phys., 12, 709–725, doi:10.5194/acp-12-709-2012, 2012.

Stocks, B. J., Mason, J. A, Todd, J. B., Bosch, E. M., Wotton, B. M., Amiro, B. D., Flannigan, M. D., Hirsch, K. G., Logan, K. A., Martell, D. L., and Skinner, W. R.: Large forest fires in Canda, 1959-1997, J. Geophys. Res., 108, 8149, doi:10.1029/2001JD000484, 2003.

Storer, R. L. and van den Heever, S. C.: Microphysical processes evident in aerosol forcing of tropical deep convective clouds, J. Atmos. Sci., 70, 430–446, doi:10.1175/JAS-D-12-076.1, 2013.

Tao, W.-K., Li, X., Khain, A., Matsui, T., Lang, S., and Simpson, J.: Role of atmospheric aerosol concentration on deep convective precipitation: cloud-resolving model simulations, J. Geophys. Res., 112, D24S18, doi:10.1029/2007JD008728, 2007.

Textor, C., Graf, H.-F., Herzog, M., Oberhuber, J. M., Rose, W. I., and Ernst, G. G. J.: Volcanic particle aggregation in explosive eruption columns part II: numerical experiments, J. Volcanol. Geoth. Res., 150, 378–394, 2006.

Trentmann, J., Luderer, G., Winterrath, T., Fromm, M. D., Servranckx, R., Textor, C., Herzog, M., Graf, H.-F., and Andreae, M. O.: Modeling of biomass smoke injection into the lower stratosphere by a large forest fire (Part I): reference simulation, Atmos. Chem. Phys., 6, 5247–5260, doi:10.5194/acp-6-5247-2006, 2006.

Tupper, A., Textor, C., Herzog, M., Graf, H.-F., Richards, M. S.: Tall clouds from small eruptions: the sensitivity of eruption height and fine ash content to tropospheric instability, Nat. Hazards, 51, 375–401, doi:10.1007/s11069-009-9433-9, 2009.